Electrical conductivity of hot expanded aluminum: Experimental measurements and *ab initio* calculations

Vanina Recoules,* Patrick Renaudin, Jean Clérouin, Pierre Noiret, and Gilles Zérah
Département de Physique Théorique et Appliquée, CEA/DAM Île-de-France, Boîte Postale 12, 91680 Bruyères-le-Châtel Cedex, France
(Received 23 April 2002; revised manuscript received 1 August 2002; published 26 November 2002)

Experimental measurements and theoretical calculations of the electrical conductivity of aluminum are presented in the strongly coupled partially degenerate regime ($\rho=0.3$ g/cm^3, $5000<T<15\,000$ K). The experiments were performed in an isochoric plasma closed vessel designed to confine electrical plasma discharges up to 1.5 GPa. Aluminum properties were determined theoretically by *ab initio* molecular dynamics simulations in the local density approximation, from which the conductivity was computed using the Kubo-Greenwood formula. The theoretical results were validated in the dense coupled regime against previously published experimental results and then applied to our experimental low density regime, showing that the theoretical results overestimate the experimental conductivities.

DOI: 10.1103/PhysRevE.66.056412 PACS number(s): 52.25.−b, 52.65.−y, 52.50.−b, 52.70.−m

I. INTRODUCTION

There is growing interest in the exploration of transport properties of strongly coupled (SC) partially degenerate plasmas, which are encountered in astrophysics, laser-produced plasma studies, or exploded wire experiments in connection with intense x-ray generation [1]. This regime, also referred to as warm dense matter, opens a challenging field for both experiments and *ab initio* simulations.

Most experimental attempts to reach the SC regime are based on heating provided by an electrical discharge or by an intense laser pulse. Plasma created by a fast electrical discharge can be confined by a capillary lead glass tube [2] or by embedding the exploding wire in water [3,4]. For laser heating experiments, aluminum samples can be tamped with transparent layers [5]. A third way to study SC plasmas is to use an electrically created quasistatic isochore plasma in a confined vessel. This is realized in an isochoric plasma closed vessel (enceinte à plasma isochore: EPI). In the EPI device, the plasma is kept in a constant volume channel during a slow electric discharge (250 μs). The confinement is realized here by the mechanical properties of the chamber and the plasma phase can be considered almost isochoric. This allows direct measurements, in one electrical discharge, of mass density, input energy, and electrical conductivity [6].

From the theoretical point of view, there are many models that predict the electrical conductivity, using various assumptions about electronic and ionic structure. In the partially degenerate SC regime those quantities are difficult to obtain because the interaction is screened by the electronic polarization and up to now there has been no correct model to account for nonlinear screening. *Ab initio* molecular dynamics is ideally suited for this type of problem, precisely because no adjustable parameters or empirical interionic potentials are needed. The energetics of the system and the forces on the ions are calculated by first-principles quantum methods and the leading ionic structure is consistent with the degeneracy of the electrons. This method has been successfully used on liquids [7–10]. We are presenting here an implementation of an *ab initio* evaluation of the electrical conductivity in order to compute properties of a SC partially degenerate plasma corresponding to the experimental density obtained in the EPI ($\rho=0.3$ g/cm^3). This represents the application of *ab initio* simulations and computation of the electrical conductivity in a diluted metallic system. In order to verify our implementation of the method, we will first present results in the dense degenerate regime ($\rho=2$ g/cm^3, $1000\ \mathrm{K}<T<15\,000$ K) where experimental results and computational estimations are available.

This paper is organized as follows. In the next section, we will describe the experimental setup. In the third part, the *ab initio* simulations are introduced, and the Kubo-Greenwood formulation is recalled and generalized to nonlocal pseudopotentials. In the last part, the method is checked against previous results (theoretical and experimental) at high density and then applied to our experiments.

II. EXPERIMENTAL SETUP

Experiments were performed in the EPI, where a metallic sample at normal density and room temperature is turned into a plasma with a known density, passing through liquid and vapor phases. The choice of the plasma density is given by the current technical possibilities of the chamber: temperature and pressure must be lower than 40 000 K and 1.5 GPa, respectively, to ensure an efficient confinement without loss of energy.

A schematic diagram of the experimental setup is shown in Fig. 1. The EPI combines two techniques: a high pulse power bank to obtain a heating of the metallic sample and a high-pressure closed vessel. The body of the vessel consists of an alternate stack of autofrettaged metallic rings (1 cm thickness) and electrical insulator Kapton foils (125 μm). The maximal pressure (1.5 GPa) is limited by the sealing performance of the Kapton foil. A sapphire ring is inserted into the center of each high-pressure ring forming, once stacked, a tube of 20 cm in length and 1.2 cm in diameter. Sapphire is a good thermal insulator. It sustains high pressure

*Electronic address: vanina.recoules@cea.fr

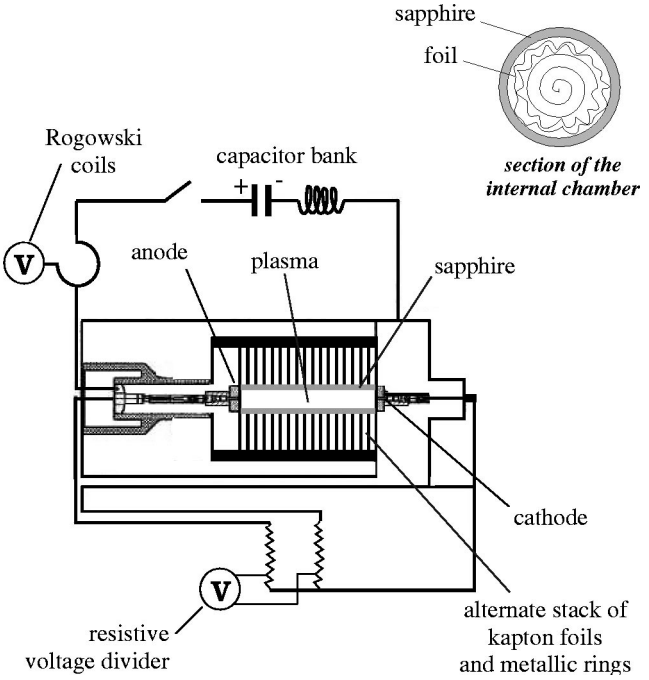

FIG. 1. Experimental setup of the EPI device.

very well and is transparent to wavelengths from 0.2 to 5 μm. The external surface of the sapphire is coated with aluminum to confine the plasma radiation by a mirror reflection. A 25 μm thick pure aluminum foil at normal density and room temperature is placed inside the vessel with a shape that fills the internal volume (see Fig. 1). This foil is in contact at each end with an electrode, of the same metal as the foil. We use a slow capacitor bank charged to an energy of 225 kJ to produce a current, which rises to a peak of 180 kA in 150 μs (see Fig. 2). Current is driven from four capacitors connected in parallel, totaling 2.42 mF, and is switched by a pressurized spark gap switch. The internal inductance of the circuit without the foil is 6 μH, which is very large in comparison with that of the foil (0.4 μH). With this experimental setup, the sample is heated for four 400 μs. The plasma volume is controlled mechanically by the closed-vessel walls.

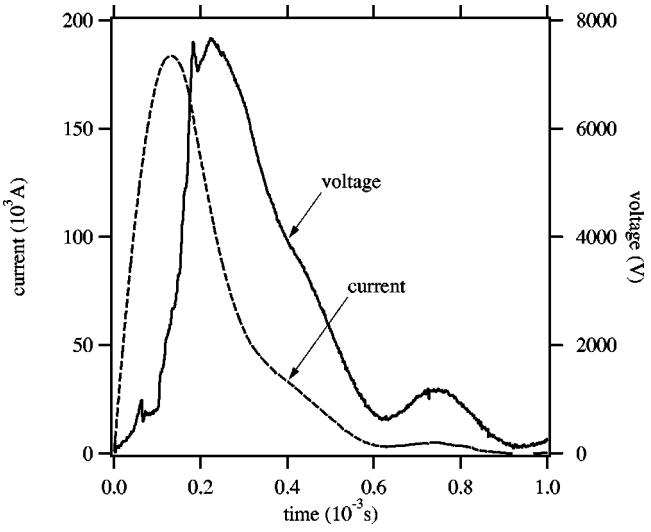

FIG. 2. Measurement of the current (dashed line) and voltage (solid line) as a function of time.

The characteristic time of the pulse-power supply is long enough to allow the formation of a homogeneous plasma, and short enough to limit the effects of wall ablation, which are supposed to be negligible during the plasma heating. The assumption of homogeneity is supported by different theoretical arguments.

(1) The duration of the energy input is about 100 μs and the sound-propagation time across a 0.6 cm thick ionized vapor of aluminum is about 3 μs, according to Ref. [11].

(2) At 10 000 K, the diameter of a free burning arc at equilibrium, dissipating the same power as in our experiment, is 2.5 cm, which is twice the inner diameter of the vessel.

(3) The skin depth δ of a conductor having the same resistivity as the plasma, at a frequency f of 5 kHz (bandwidth derived from a Fourier transform analysis of the current signal) with conductivity σ and permeability μ is given by

$$\delta = \sqrt{\frac{1}{\pi f \sigma \mu}} \tag{1}$$

and is six times as large as the inner radius of the vessel.

(4) The magnetic pressure for a 100 kA current in a 1.2 cm diameter cross section is about 30 MPa, which is small compared to the 1 GPa reached in the vessel during the experiment.

Since the plasma is homogeneous, the density depends only on the initial mass of the material placed in the vessel. A total mass of aluminum of 6.7 g leads to an average density of 0.3 g/cm^3. A Rogowski belt surrounds one electrode to measure the time derivative of the current and a resistive divider is used to measure the voltage drop across the plasma. The time derivative dI/dt of the current and the inductance L of the plasma (0.4 μH) are small enough to make the $L \times dI/dt$ term negligible compared to the measured voltage, except at the very beginning of the discharge. Therefore, no inductive correction is needed to obtain the plasma resistivity from the current and voltage measurements (shown in Fig. 2).

At each shot, the input energy and the electrical resistivity of the plasma are inferred from the current and voltage measurements. The resistivity of the plasma is determined by using the relation $\rho(t) = \pi r^2(t) R(t)/l(t)$ where the length $l(t)$ and the radius $r(t)$ of the plasma are the length and the inner radius of the vessel, respectively. The uncertainty in current and voltage measurements produces a 15% uncertainty in the resistance of the plasma. The internal energy variation δU can be evaluated from the electrical energy input E_{el} and is given by $\delta U = (E_{el} - E_{rad}) + \delta W$, where E_{rad} are the thermal losses at the vessel walls. The mechanical work loss δW due to the vessel expansion under pressure is less than 1% of E_{el} and can be neglected. The thermal losses are assumed to be radiative during the plasma phase, and negligible before. The internal energy is obtained at each

time by resolving the following differential equation: $dU/dt = dE_{el} - \alpha\sigma_0 S T(U)^4$, where σ_0 is the Stefan-Boltzmann constant, S is the plasma surface and T is written as a function of U using the SESAME tables [11]. Because of the isochoric and monophasic assumption, the maxima of internal energy, electrical conductivity, and pressure are reached at the same time. At this time, α is measured and depends only on the instantaneous power dE_{el}/dt.

III. *AB INITIO* CALCULATIONS

The most general formulation for computing the electrical conductivity is given by the Kubo-Greenwood formulation in which no particular assumptions are made on the ionic structure or on the electron-ion interactions. In the framework of the quasi-independent particule approximation, the Kubo-Greenwood expression [12,13] in the linear response theory yields the real part of the optical conductivity expressed as

$$\sigma(\omega) = \frac{2\pi e^2}{3\omega} \int d\boldsymbol{k} \sum_{n,m} (f_n - f_m) \times |\langle \psi_n | \hat{\boldsymbol{v}} | \psi_m \rangle|^2 \delta(E_m - E_n - \hbar\omega), \quad (2)$$

where ω is the frequency, e is the electronic charge, ψ_n and E_n are the electronic eigenstates and eigenvalues for the electronic state n, f_n is the Fermi distribution function, and $\hat{\boldsymbol{v}}$ is the velocity operator. Calculations of the eigenstates and eigenvalues are made in the framework of density functional theory.

For disorded systems, such as liquids or plasma, density functional theory (DFT) provides a unique tool for computing electronic properties and ionic structure. DFT assumes that the ground state energy of a system of interacting electrons moving in an external potential is a unique function of the electronic density n_e [14]. For a given external potential (an ionic configuration) minimization of the electronic energy of the system yields the exact ground state (variational principle). The set of electronic orbitals ψ_n of electronic state n that minimize the Kohn-Sham energy functional is given by the self-consistent solutions to the Kohn-Sham equations [15]:

$$\left[\frac{-\hbar^2}{2m_e} \nabla^2 + V_{ion}(\boldsymbol{r}) + V_H(\boldsymbol{r}) + V_{XC}(\boldsymbol{r}) \right] \psi_n(\boldsymbol{r}) = E_n \psi_n(\boldsymbol{r}), \quad (3)$$

where E_n are the Kohn-Sham eigenvalues, $V_{ion}(\boldsymbol{r})$ is the static total electron-ion potential, $V_H(\boldsymbol{r})$ is the Hartree potential, and $V_{XC}(\boldsymbol{r})$ is the exchange and correlation potential. These Kohn-Sham equations are a set of eigenequations, and the terms within the square brackets can be regarded as a Hamiltonian. The exchange and correlation term is not exactly known. It is approximated by the local density approximation (LDA) based on the exact result for a homogeneous electron gas, and the generalized gradient approximation which accounts for density gradients. Only the valence electrons are treated explicitly, the interaction between the valence electrons and the atomic cores being represented by pseudopotentials. For systems at a temperature close to the Fermi temperature ($\theta \simeq 1$), DFT can be extended to a finite temperature, as shown by Mermin, and the variational principle still holds with the electronic free energy [16]. This finite temperature functional procedure provides a highly accurate determination of the forces that operate on ions. Electronic orbitals are populated according to a the Fermi-Dirac distribution. In contrast with the zero temperature case where states beyond the Fermi level are empty, a large number of excited states must be considered. The molecular dynamics generalization of the method that was previously introduced by Car and Parrinello is now realized by a step by step minimization using efficient algorithms.

All of our simulations use constant density and volume. We use a finite sample in a basic cubic reference cell, with a finite number of electrons. We also invoke periodic boundary conditions. Simulation of periodic systems introduces the question of Brillouin zone sampling. Methods have been devised for obtaining very accurate approximations to the electronic potential and the contribution to the total energy from electronic orbitals by calculating the electronic states at special $\boldsymbol{k}$ points in the Brillouin zone (BZ). For large disorded systems, this constraint become less compelling and simulations at the Γ point can be used. The electrical conductivity and more generally optical properties are very sensitive to a detailed description of the electronic density. In particular, a correct BZ sampling is necessary to obtain accurate results. This observation led us to use a two-step procedure.

First, ionic structures are generated with the *ab initio* code VASP developed by Kresse and Hafner [17], in which ion-electron interactions are described with Vanderbilt ultrasoft pseudopotentials [18]. The Perdew and Wang parametrization of the generalized gradient approximation [19] is used for the exchange and correlation potential. The generation of atomic structures is done at the Γ point and is performed for 32 or 108 atoms for 300–500 time steps of 2 fs after equilibration without thermostat (pure microcanonical). We consider electronic states occupied down to 10^{-6}.

In a second step, for selected statistically independent atomic configurations, a self-consistent ground state calculation is performed with the ABINIT code [20,21] to get the detailed electronic structure. The electronic calculation is done in the local density approximation with the Ceperley-Adler [22] exchange-correlation energy as parametrized by Perdew and Wang [23]. The pseudopotential used in our work is generated by the method of Troullier and Martins [24]: $3s$ and $3p$ states are treated as valence electrons and we use a d nonlocal part. Orbitals are expanded in plane waves up to a cutoff of 12 Ry. The Brillouin zone was sampled with the Monkhorst-Pack scheme [25] and convergence in $\boldsymbol{k}$ vectors was tested. We find that, for simulations with 108 atoms, convergence is reached with the usage of four special $\boldsymbol{k}$ points. With increasing temperature, it appears that electronic structure is less sensitive to the number of $\boldsymbol{k}$ points and to the number of atoms in the cubic cell. Moreover, to compute optical properties we need to introduce unoccupied excited states. For high density, between 250 (for $T = 1000$ K) and 500 orbitals (for $T = 15000$ K) are consid-

ered for a 108-atom cubic cell. For low density, between 300 and 500 orbitals are considered for a 32-atom cubic cell.

In most publications using the Kubo-Greenwood formalism [8,9,26], the velocity operator $\hat{\boldsymbol{v}}$ is expressed as the momentum operator $\hat{\boldsymbol{p}}$. This is correct if the Hamiltonian contains only a local potential. In our case, nonlocal pseudopotentials are used and this equivalence is no longer valid. The definition of the velocity operator in the Heisenberg representation,

$$\hat{\boldsymbol{v}} = \frac{i}{\hbar}[\hat{H}, \boldsymbol{r}], \tag{4}$$

must be used. $\hat{H}$ represents the total Hamiltonian of the system. Then, $\hat{\boldsymbol{v}}$ is expressed in terms of $\partial\hat{H}/\partial\boldsymbol{k}$. The integration in the BZ is replaced by a summation over special $\boldsymbol{k}$ points:

$$\sigma(\omega) = \frac{2\pi e^2}{3\omega}\frac{1}{\Omega}\sum_{\boldsymbol{k}} W(\boldsymbol{k}) \sum_{n,m} (f_n^{\boldsymbol{k}} - f_m^{\boldsymbol{k}}) \times \frac{1}{(2\pi^2)} \left| \left\langle \psi_n^{\boldsymbol{k}} \left| \frac{\partial\hat{H}}{\partial\boldsymbol{k}} \right| \psi_m^{\boldsymbol{k}} \right\rangle \right|^2 \delta(E_m^{\boldsymbol{k}} - E_n^{\boldsymbol{k}} - \hbar\omega), \tag{5}$$

where $W(\boldsymbol{k})$ is the $\boldsymbol{k}$-point weight in the Monkhorst-Pack scheme. Technical details of the computation of the matrix elements $\langle \psi_n^{\boldsymbol{k}} | (\partial\hat{H}/\partial\boldsymbol{k}) | \psi_m^{\boldsymbol{k}} \rangle$ can be found in Refs. [27,28]. The δ function can be resolved by averaging over a finite frequency interval $\Delta\omega$ [29]:

$$\sigma(\omega_l) = \frac{1}{\Delta\omega}\int_{\omega_l - \Delta\omega/2}^{\omega_l + \Delta\omega/2} \sigma(\omega)\, d\omega. \tag{6}$$

Introducing Eq. (6) in Eq. (5) eliminates the δ function and yields a simple sum over states. The above formulas apply for an ionic configuration at a single time step within a molecular dynamics trajectory. Optical properties are calculated for selected configurations until convergence is reached.

The conductivity $\sigma(\omega)$ must satisfy the sum rule [12]

$$S = \frac{2m_e\Omega}{\pi e^2 n_e}\int_0^{\infty} \sigma(\omega)\, d\omega = 1, \tag{7}$$

where m_e is the electron mass and n_e the electronic density. Since a finite number of excited states is included in the calculation, $\sigma(\omega)$ is computed correctly for $\hbar\omega < |E_{\max} - E_{\mathrm{f}}|$ where E_{f} is the Fermi level and $E_{\max}$ is the energy of the highest level computed. To obtain a well converged sum rule, we need to introduce more unoccupied electronic states than for the determination of the dc electrical conductivity $\sigma(\omega \to 0)$. The dc electrical conductivity σ_{dc} computation is made by extrapolating the optical conductivity to $\omega = 0$. In our calculations S is always smaller than 1.

IV. RESULTS

The plasma phases can be characterized by the ion-ion coupling parameter Γ which is the ratio of the mean electrostatic potential energy to the mean kinetic energy: $\Gamma = \overline{Z}^2 e^2/(4\pi\epsilon_0 k_B T a)$, where e is the electronic charge, ϵ_0 is the vacuum dielectric constant, k_B is the Boltzmann constant, T is the temperature, $a = (4/3\pi n_i)^{-1/3}$ is the mean ion-sphere radius, and n_i is the ionic number density. $\overline{Z}$ is the average ionization degree of atoms, which depends on the density and temperature conditions. The plasma is said to be strongly coupled when this ratio is greater than 1.

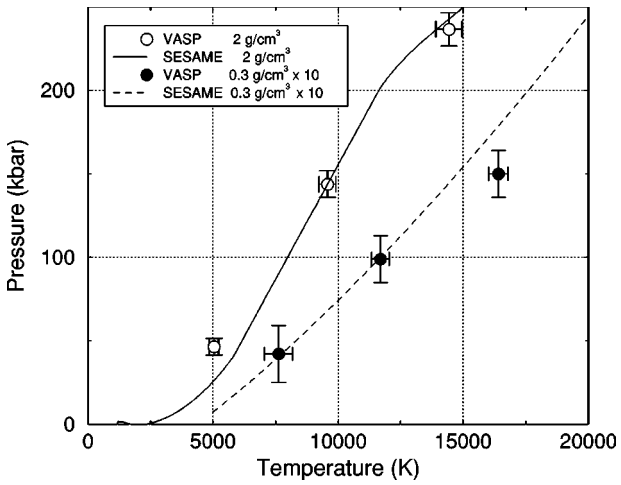

FIG. 3. Pressure as a function of temperature for two densities: $\rho = 2$ g/cm^3 and $\rho = 0.3$ g/cm^3 (multiplied by a factor of 10).

The electronic degeneracy parameter θ is the ratio of the temperature to the Fermi temperature T_F. If $n_e = \overline{Z} n_i$ is the electronic density in cm^{-3} and T the temperature in K, $\theta = T/T_F = 2.29 \times 10^{10} T n_e^{-2/3}$. When $\theta \to 0$, the electrons are fully degenerate, which is the case for a metal under normal conditions. The first case presented below ($\rho = 2$ g/cm^3) enters into this category, whereas the low density case ($\rho = 0.3$ g/cm^3) can be regarded as partially degenerate.

A. Dense degenerate regime ($\rho = 2$ g/cm^3)

As mentioned in Sec. II, we first performed *ab initio* simulations with the VASP code using 108 particles at three temperatures (1000 K, 5000 K, and 15 000 K). Trajectories are generated for 500 time steps of 2 fs at the Γ point. The equation of state (pressure versus temperature) obtained from the molecular dynamic simulations is shown in Fig. 3. The equation of states deduced from the SESAME tables [11] is shown too.

In order to check our implementation of the method, we compute the electrical conductivity at a density of 2 g/cm^3 representative of expanded liquid aluminum. From the molecular dynamics simulation done at the Γ point, the electronic structure is computed for five statistically independent configurations with four $\boldsymbol{k}$ points. The densities of states (DOS's) for the three temperatures are presented in Fig. 4. As expected for this regime, they show a free-electron-like behavior at all temperatures. There is neither a gap nor a minimum near the Fermi level.

The real part of the optical conductivity is plotted in Fig. 5. Each curve is the result of the conductivity averaged over five ionic configurations statistically independent for the

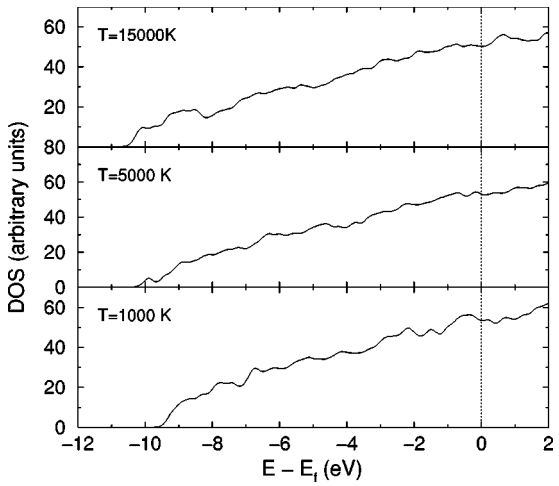

FIG. 4. Density of states for three temperatures $T=1000$ K, $T=5000$ K, and $T=15\,000$ K at $\rho=2$ g/cm^3.

three temperatures considered. For all temperatures, the sum S is equal to 0.9 showing that the convergence of electronic structure is sufficient for the evaluation of the dc electrical conductivity.

The extrapolation to zero frequency must be performed carefully since in a finite system energy levels are always discrete and $\sigma(\omega)$ falls to zero for small values of ω [8]. Therefore, it is more convenient to use a functional form for extrapolating to zero. A natural functional form for fitting the calculated $\sigma(\omega)$ in this regime would be the Drude formula:

$$\sigma(\omega)=\frac{\sigma_{\mathrm{dc}}}{1+\omega^2\tau^2}, \tag{8}$$

where τ is the relaxation time. The Drude formula, plotted in Fig. 5, is found to accurately reproduce the computed optical

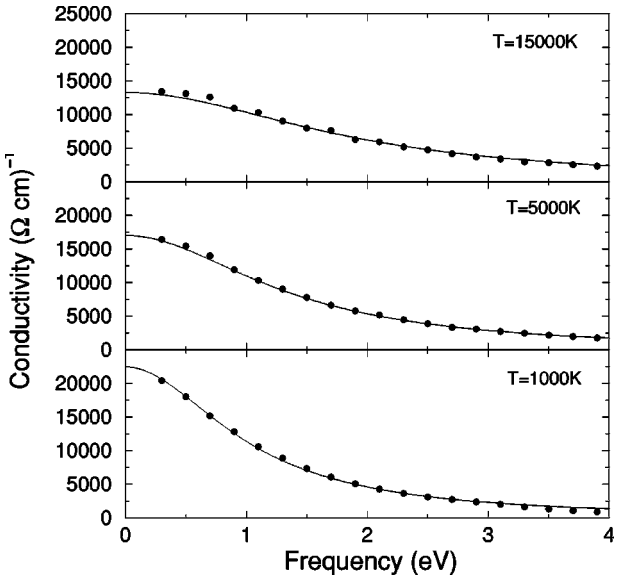

FIG. 5. Computed optical conductivities (full circles) versus frequency for three temperatures $T=1000$ K, $T=5000$ K, and $T=15\,000$ K at $\rho=2$ g/cm^3. Full lines are the Drude fits using relaxation times τ and dc conductivities given in Table I.

TABLE I. Relaxation times and dc electrical conductivities versus temperature obtained in the dense regime at $\rho=2$ g/cm^3 by the Drude fit [Eq. (8)] of the optical conductivities.

T (K)	1000	5000	15 000
τ (10^{-16} s)	6.7	4.9	3.8
σ_{dc} [$10^3(\Omega\ \mathrm{cm})^{-1}$]	23.9	17.0	14.6

conductivities, showing the metallic character of aluminum at $\rho=2$ g/cm^3. Using this fit, the zero frequency limit yields the dc conductivity (see Table I).

From the computed electrical conductivity and relaxation time, we computed the electronic density in cm^{-3} using the Drude formula

$$n_e=\frac{m_e\sigma_{\mathrm{dc}}}{\tau e^2}, \tag{9}$$

where m_e and e are the electron mass and charge. We found $1.3\pm0.05\times10^{23}$ cm^{-3} for the three considered temperatures. On the other hand, the electronic density in the cubic cell, considering three valence electrons, is 1.27×10^{23} cm^{-3}. This shows that the ionization deduced from the Drude approach is equal to three. Using this average ionization, we compute the coupling parameter $\Gamma\simeq50$ for $T=15\,000$ K. It is about 170 for $T=5000$ K. The degeneracy parameter is nearly 0.1 for all temperatures.

The electrical conductivity as a function of temperature is plotted in Fig. 6, and is compared to the highest density reached in the experiments of Benage *et al.* [2] at about $T=15\,000$ K and of Mostovych and Chan at about $T=5000$ K [5]. The electrical conductivity decreases with increasing temperature, as expected for a metal. This is in agreement with the calculated density of states. At high temperature, our results are very close to the experimental results of Ref. [2] for $T=15\,000$ K. At $T=5000$ K, our theoretical

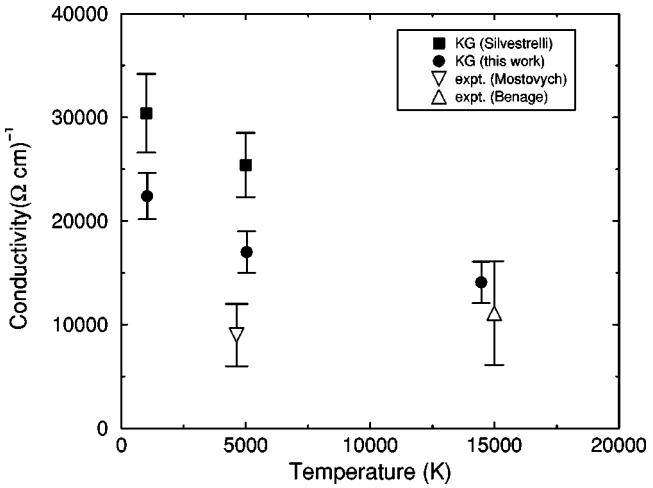

FIG. 6. Electrical dc conductivity versus temperature at $\rho=2$ g/cm^3. Our model (full circles) is compared with simulations of Silvestrelli (full square, [8]) and with the experiments of Ref. [2] (up triangle) and [5] (down triangle).

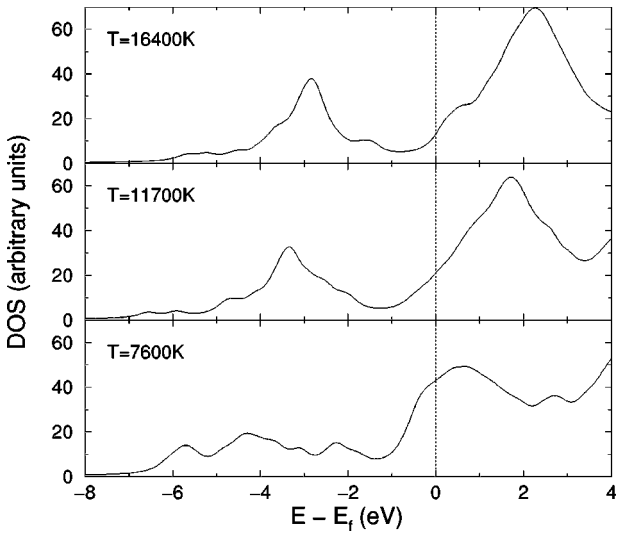

FIG. 7. Density of states for three temperatures $T=7\ 600$ K, $T=11\ 700$ K, and $T=16\ 400$ K at $\rho=0.3$ g/cm^3.

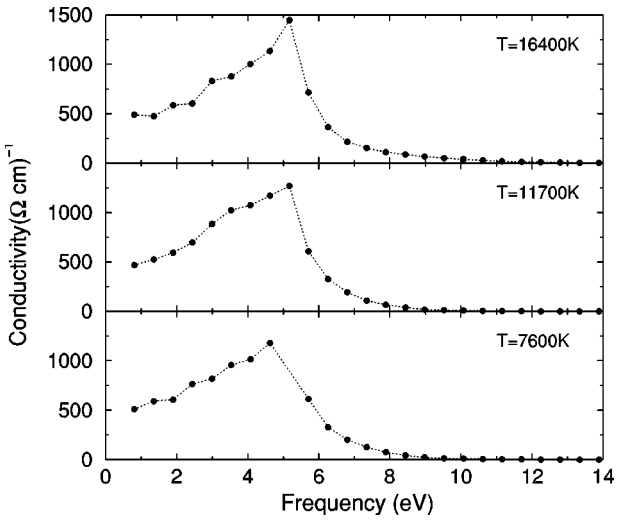

FIG. 8. Optical conductivities versus frequency for three temperatures $T=7600$ K, $T=11\ 700$ K, and $T=16\ 400$ K at $\rho=0.3$ g/cm^3. Dashed lines are here to guide the eyes.

estimations are in better agreement with the experimental results of Mostovych and Chan [5] than the theoretical predictions of Silvestrelli [8]. This discrepancy between the two theoretical results can be traced back to the fact that Silvestrelli used the momentum operator in the Kubo-Greenwood formula instead of the velocity operator in the Heisenberg representation. The nonlocal contributions, which are accounted for in our calculations, are probably greater than expected even in this regime [30]. We conclude that our implementation of Kubo-Greenwood formulation is satisfactory.

B. Partially degenerate regime ($\rho=0.3$ g/cm^3)

Using the same procedure, we generate ionic configurations representative of the plasma created in the EPI ($\rho=0.3$ g/cm^3). It must be noted that such a small density is much more demanding in computer resources than the previous case because of a bigger simulation box and, consequently, the number of plane waves to be computed. This is why micro-canonical simulations are performed for only 32 atoms, for 300 time steps after equilibration for $T=7600$ K, 11 700 K, and 16 400 K. As in the previous case, the optical analysis is derived afterwards from selected ionic configurations.

The DOS's shown in Fig. 7 are very different from those at a higher density. We no longer observe a free-electron-like form and a structure appears in the DOS. One remaining limitation of the plane wave technique is that the extended basis set does not provide a natural way of quantifying local atomic properties. One can hardly extrapolate the nature of the peak of the DOS and only some general trends can be drawn. As the temperature increases, states become more localized. The band centered on ~ -3 eV is due to the $3s$ electrons and the shoulder around ~ -2 eV is due to the $3p$ electrons.

Clearly, the optical conductivities, plotted versus frequency on Fig. 8 are no longer characteristic of a simple free electron Drude metal but are more reminiscent of nonmetallic systems [7,26]. The sum rule has the value of 0.9, which is satisfactory to compute the dc electrical conductivity. In view of the difference in the density of states between the two densities, it is not surprising to find that the electrical conductivity changes dramatically. There is a peak around 5 eV which might be a result of transitions between the bands at ~ 3 eV below the Fermi level of $3s$ character and the unoccupied states with energies ~ 2 eV above the Fermi level of $3p$ character.

Table II presents the theoretical results of molecular dynamics (MD) and the experimental measurements. This allows a direct comparison between theoretical and experimental results. As shown in Table II, there is a slight increase of conductivity versus internal energy variation.

The electrical conductivity is plotted as a function of temperature in Fig. 9. For the experimental points obtained in the EPI, the temperature is deduced from the internal energy variation using the SESAME tables [11]. The vertical error bars indicate the uncertainty in the conductivity measurements. The temperature uncertainty is assumed to be equal to the electrical energy uncertainty, i.e., 15%. Other experimental results obtained from [3,4] have been added in Fig. 9 and

TABLE II. Computed temperature, internal energy variation, pressure, and dc electrical conductivity of aluminum at $\rho=0.3$ g/cm^3, and experimental internal energy variation and conductivity. For the computed internal energy variation, the reference energy is the internal energy of solid density at room temperature.

	T (K)	ΔU_{int} (MJ/kg)	P (kbar)	$\sigma(\Omega\ \text{cm}^{-1})$
	7600	12.9	4.0	460.0
M.D.	11 700	17.0	9.9	480.0
	16 400	19.3	15.0	520.0
	24 800	37.0	31.0	700.0
Expt.		22.0		207.0

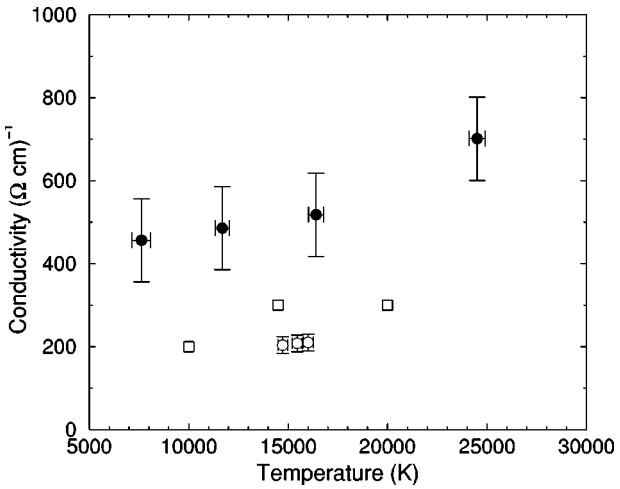

FIG. 9. Electrical dc conductivity (full circles) versus temperature at $\rho=0.3$ g/cm^3 compared with our experimental data (open circles) and with those of Refs. [4].

are in rather good agreement with our experimental data. For the theoretical conductivities, the extrapolation to zero frequency is much more difficult due to the statistical noise of the optical spectra at low frequency, leading to large error bars in Fig. 9. The extrapolation is done using a cubic regression on the fourth first point. The order of magnitude of the conductivity is characteristic of a semiconductor. The dependency of the electrical conductivity on temperature is different from that in the high density case (see Fig. 6). The slight increase in temperature is in accordance with the experimental results.

The average ionization was estimated using the average atom model SCAALP [6] for $\rho=0.3$ g/cm^3 and $T=15\,000$ K. In these conditions, the fraction of electrons having their energy level beyond the Fermi level is equal to 1.25. Following this, and using Fermi-Dirac occupations, we computed a number of electrons of 1.23, in excellent agreement with the SCAALP prediction.

This average ionization leads to a coupling parameter $\Gamma=5$ and a degeneracy parameter of $\theta=0.9$, characteristic of a SC partially degenerate plasma [31]. For the three higher temperatures, the coupling parameter is between 4 and 5 whereas for $T=7600$ K it is about 0.6 (lower than 1).

V. CONCLUSION

To summarize, we have carried out an experiment directly measuring electrical resistivity, mass density, and internal energy variation of a strongly coupled aluminum plasma. We stress that all the above mentioned quantities are measured in an absolute way, without any external models.

Then we showed a calculation of electronic structure and conductivity for aluminum at $\rho=2$ g/cm^3 and $\rho=0.3$ g/cm^3 using *ab initio* molecular dynamics. The electrical conductivity was computed using the Kubo-Greenwood formula. Simulations gave reasonnably good results compared to the experiments at $\rho=2$ g/cm^3 in a regime where the system is correlated and degenerate. The use of the velocity operator defined in the Heisenberg representation improves the computational results compared to those using the momentum operator. In the partially degenerate regime $\rho=0.3$ g/cm^3, the theoretical result overestimates the experimental conductivities.

The fact that the plasma is partially degenerate ($\theta=0.7$) indicates that the temperature is close to the Fermi temperature and consequently that finite temperature effects are no longer negligible. This is accounted for by the Mermin functional. To be fully consistent, a temperature dependent functional form for the exchange and correlation term should be used, and this could improve our results [6,32,33].

The calculation of the DOS and optical properties using DFT relies on a calculation of the Kohn-Sham eigenvalues with the real eigenfunctions. Then, the use of Kohn-Sham eigenvalues to estimate the excitation spectrum might be questionable [34]. Moreover, in practice, the exact functional is not known and approximations such as the LDA must be used. This results in an approximate Hamiltonian and additional errors in the Kohn-Sham eigenvalues and eigenfunctions. The well-known band gap underestimation when computed in LDA [35] affects optical properties for small ω and leads to very high electrical conductivity. In a metallic system with no gap, the error is probably small, which explains why our results are in better agreement with experiment for the higher density showing a metallic DOS. The introduction of quasiparticle energy can improve the DFT-LDA results for the partially degenerate regime.

ACKNOWLEDGMENTS

We gratefully acknowledge S. Bernard for supplying the pseudopotential, M. Torrent, F. Jollet, X. Gonze, and S. Mazevet for useful discussions, and B. Loffredo and M. Sonnaert for their technical assistance during the course of this work.

[1] A good review is found in Contrib. Plasma. Phys. 41 2001.
[2] J.F. Benage, W.R. Shanahan, and M.S. Murillo, Phys. Rev. Lett. **83**, 2953 (1999).
[3] A.W. De Silva and J.D. Katsouros, Phys. Rev. E **57**, 5945 (1998).
[4] I. Krisch and H.J. Kunze, Phys. Rev. E **58**, 6557 (1998).
[5] A.N. Mostovych and Y. Chan, Phys. Rev. Lett. **79**, 5094 (1997).
[6] P. Renaudin, C. Blancard, G. Faussurier, and P. Noiret, Phys. Rev. Lett. **88**, 215001 (2002).
[7] L.A. Collins, S.R. Bickham, J.D. Kress, S. Mazevet, T.J. Lenosky, N.J. Troullier, and W. Windl, Phys. Rev. B **63**, 184110 (2001).
[8] P.L. Silvestrelli, Phys. Rev. B **60**, 16 382 (1999).

[9] J.M. Holender, M.J. Gillan, M.C. Payne, and A.D. Simpson, Phys. Rev. B **52**, 967 (1995).
[10] G. Galli, R.M. Martin, R. Car, and M. Parrinello, Phys. Rev. Lett. **63**, 988 (1989).
[11] Los Alamos National Laboratory Report No. LA-UR-92-3407, 1992, edited by S.P. Lyon and J.D. Johnson (unpublished).
[12] R. Kubo, J. Phys. Soc. Jpn. **12**, 570 (1957).
[13] D.A. Greenwood, Proc. Phys. Soc. London **715**, 585 (1958).
[14] P. Hohenberg and W. Kohn, Phys. Rev. **136**, B864 (1964).
[15] W. Kohn and L.J. Sham, Phys. Rev. **140**, A1133 (1965).
[16] N.D. Mermin, Phys. Rev. **137**, A1441 (1965).
[17] G. Kresse and J. Hafner, Phys. Rev. B **47**, 558 (1993).
[18] D. Vanderbilt, Phys. Rev. B **41**, 7892 (1990).
[19] J.P. Perdew, *Electronic Structure of Solids* (Akademie-Verlag, Berlin, 1991).
[20] ABINIT code is a common project of the Université Catholique de Louvain, Corning Incorporated, CEA and other contributors, URL http:/www.abinit.org.
[21] M.C. Payne, M.P. Teter, D.C. Allan, T.A. Arias, and J.D. Joannopoulos, Rev. Mod. Phys. **64**, 1045 (1992).
[22] D.M. Ceperley and B.J. Alder, Phys. Rev. Lett. **45**, 566 (1980).
[23] J.P. Perdew and Y. Wang, Phys. Rev. B **33**, 8800 (1986).
[24] N. Troullier and J.L. Martins, Phys. Rev. B **43**, 1993 (1991).
[25] H.J. Monkhorst and J.D. Pack, Phys. Rev. B **13**, 5188 (1976).
[26] E. Fois, A. Selloni, and M. Parrinello, Phys. Rev. B **39**, 4812 (1989).
[27] X. Gonze, Phys. Rev. B **55**, 10337 (1997).
[28] X. Gonze and C. Lee, Phys. Rev. B **55**, 10 355 (1997).
[29] O. Pfaffenzeller and D. Hohl, J. Phys.: Condens. Matter **9**, 11 023 (1997).
[30] A. Marini, G. Onida, and R. Del Sole, Phys. Rev. B **64**, 195125 (2001).
[31] S. Ichimaru, *Statistical Plasma Physics, Vol. II: Condensed Plasma* (Addison-Wesley, Reading, MA, 1994).
[32] M.P. Suhr, T.W. Barbee III, and L.H. Yang, Phys. Rev. Lett. **86**, 5958 (2001).
[33] F. Perrot and M.W.C. Dharma-Wardana, Phys. Rev. B **62**, 16 536 (2000).
[34] F. Kirchhoff, J.M. Holender, and M.J. Gillan, Phys. Rev. B **54**, 190 (1996).
[35] L.J. Sham and M. Schlüter, Phys. Rev. Lett. **51**, 1888 (1983).